

الهيئة الليبية للبحث العلمي

Libyan Authority For Scientific Research



 $\ln^n(x)dx$ 

**TINNS** 

# Libyan International Journal of Natural Sciences

**VOLUME 1 ISSUE NO 1 MAY 2025** 

Bi-Annual, Peer- Reviewed, and Open Accessed e-Journal

















## **Libyan International Journal of Natural Sciences (LIJNS)**

Vol.1 Issue No 1 May 2025



### Influence of Thermal Treatment on the Structural and Morphological Properties of Intrinsic and CuO/Al-Doped Nanoparticles

<sup>1\*</sup> F. N. Zaggout D, Physics Department, Faculty of Science, Misurata University, Misurata, Libya F. A. Aljabou, Physics Department, Faculty of Science, Misurata University, Misurata, Libya

#### ARTICLE INFORMATION

#### Article history:

Received 04 April 2025 Accepted 03 May 2025 Published 07 May 2025

#### **Keywords:**

Al doped CuO. XRD. AFM. Nanoparticles. Nanorods.

Nanowires.

Nanotubes.

#### **ABSTRACT**

In this work, pure and Al-doped CuO nanocrystalline material is prepared employing the Sol-Gel method. The pure and doped samples are heated to temperatures up to 600°C. The effect of thermal treatment on both structural and morphological properties is investigated. The structural properties are studied using the XRD technique. The results show that the pure and Al-doped CuO powders have a monoclinic structure with two preferred orientations, (002) and (200). The analysis indicates a slight shift of the prevailing crystallization peaks towards higher diffraction angles due to the doping effect and the thermal treatment. It also shows that peak intensity increases with Al doping. Additionally, the impact of heat treatment on both pure CuO and CuO/Al on crystallite size, inter-planar distance, and dislocation density is further investigated. The surface morphology is investigated using the AFM technique. AFM images have shown the formation of interesting organized nanoparticles for the first time, their shape changes from semi-spherical to oval to cylindrical rods within the nanoscale dimensions. Moreover, the intrinsic nanorods are converted to nanotubes by thermal oxidation at ambient air conditions. Therefore, this study confirms the simplicity of converting metal oxide nanorods to nanotubes through thermal oxidation under ambient air conditions.

©Author(s) 2025. This article is distributed under the terms of the CC BY-NC 4.0.

#### 1. Introduction

Copper oxide (CuO) nanoparticles, a subclass of metal oxide nanomaterials, have attracted considerable research interest due to their distinctive physicochemical properties and diverse applications. As a p-type semiconductor, CuO exhibits an indirect band gap ranging from 1.0 to 2.08eV and crystallizes in a monoclinic structure [1,2]. Notably, CuO nanoparticles can be synthesized in various morphological forms, including particles, spheres, flowers, and rods [3]. Synthesis methods for CuO nanoparticles include chemical, physical, and biological approaches, each influencing their size, morphology, and overall properties [1-3]. Every application of CuO nanostructured materials requires specific physicochemical properties, significantly influenced by the nanostructure and growth processes. To achieve the goal of obtaining nanoparticles with suitable properties for many applications, several researchers have reported different synthesis techniques that have been used to fabricate CuO nanomaterials, such as solid-state reaction. sol-gel, hydrothermal, solvothermal, thermal oxidation, pyrolysis, and sonochemical methods.

Because of the doping effect on the physical properties of semiconductors, effective efforts have been made recently to examine the effects of element doping on the structural, electrical, and optical properties of CuO nanoparticles. Different dopants, such as Ce, Ni, Pb, Zn, Cd [4], and Al, have been used [5]. Ponnar et al. [6] demonstrated the synthesis of Ce-doped CuO nanostructures, revealing a transition in microstructure from spherical to rod-like shapes, accompanied by a variation in the optical band gap from 3.63eV to 3.13eV. Similarly, Mersian et al. [7] investigated the effect of Zr doping on the structural and antibacterial properties of CuO synthesized using the Pechini method, observing improved antibacterial activity due to Zr incorporation. Thangamani et al. [8] reported the synthesis of pure and Ni-doped CuO nanostructures, noting changes in lattice parameters and optical band gap values ranging from 3.21eV to 3.10eV for spherical nanostructures. Saleem et al. [3] studied the optical and electrical properties of pure CuO and Zn-doped CuO nanoparticles for optoelectronic devices. This study suggested that Zn<sup>2+</sup> is a more efficient substitute for CuO than other transition metal ions due to the comparable ionic radii of Zn<sup>2+</sup> (0.60Å) and Cu<sup>2+</sup> (0.57Å),

<sup>\*</sup> Corresponding author: E-mail addresses: fnzaggout@sci.misuratau.edu.ly

respectively. The findings showed that the average crystalline size ranged from 25.23nm to 21.18nm, lattice constants ranged between 7.893Å and 7.745Å, and dislocation density was  $(1.57-2.22)\times10^{15}$  m<sup>-2</sup>. The addition of Zn increased the band gap energy from 1.47eV to 1.62eV. As a consequence, enhanced electrical resistivity from  $9.12\times10^3\Omega\cdot\text{cm}$  to  $4.84\times10^4\Omega\cdot\text{cm}$  was analyzed.

In this study, the sol-gel method has been used to prepare pure CuO and Al-doped CuO nanoparticles because it is a compelling technique for synthesizing materials. It is known to prepare nanopowders or materials with fine microstructures at low temperatures. Moreover, it ensures high chemical purity and homogeneity while controlling the morphology of the synthesized materials [9]. In addition, it is safe, simple, and low-cost. Al has been used as a dopant element due to its low cost and natural abundance. Moreover, the significant difference in ionic radii between Cu<sup>2+</sup> (0.73 Å) and Al<sup>3+</sup> (0.5 Å) is expected to cause remarkable variations in the properties of CuO nanoparticles. Pure and Al-doped CuO powders are prepared using raw materials such as copper sulfate, sodium hydroxide, and aluminum for doping purposes. Then, the pure and doped samples are heat treated at different temperatures (room temperature, 400 °C, 450 °C, 500 °C, 550 °C, 600 °C) in order to study the influence of the thermal treatment on the structural and morphological characteristics of CuO nanoparticles. The structural properties of the samples are analyzed using the XRD technique, and the morphological properties are investigated using AFM techniques.

#### 2. Experimental procedure

The preparation of copper oxide nanoparticles is based on two basic solutions: The first consists of 20 mL of deionized water to which 2g of CuSO<sub>4</sub> is added and placed in a glass beaker. The solution is mixed using a magnetic stirrer for 3 minutes at room temperature, resulting in a homogeneous solution with a concentration of 0.4 mol/L. The second solution consists of 8 g of NaOH added to 200 mL of deionized water, and mixed in the same way until the mixture becomes homogeneous. The concentration of the obtained solution is 1 mol/L.

#### 2.1 Preparation of CuO nanopowder

Pure CuO nanopowder is prepared by the Sol-Gel method as follows: the prepared solution of hydrated copper sulfate (CuSO4) is placed in a cup and the sodium hydroxide solution NaOH is added to it. The new solution is placed on a heating plate at 100 °C for 1 hour with magnetic stirring. The solution color changes to light gray and continues to change to black while forming very small grains that can be noticed, as shown in Fig. 1.

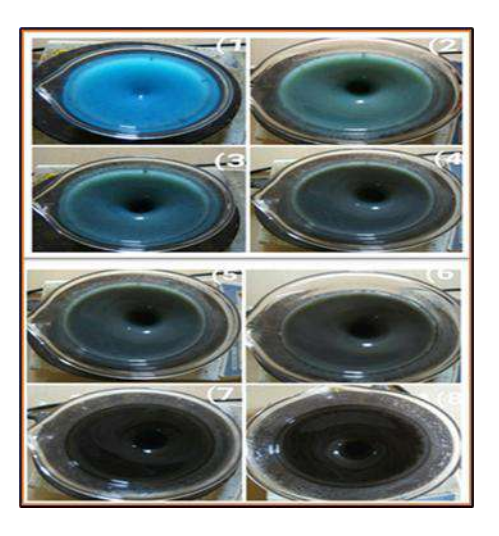


Fig. 1: Showing CuO nanoparticles' preparation.

After this heat treatment, the resulting solution is filtered. The precipitated solid is dried at a temperature of 100 °C for 1 hour, then the product is ground well with a mortar to obtain copper oxide nanopowder. The nanopowder is divided into 6 samples, which are thermally treated at different temperatures (room temperature, 400 °C, 450 °C, 500 °C, 550 °C, 600 °C). The samples are kept in the oven at the desired temperature for 1 hour and then removed to cool.

#### 2.2 Preparation of doped solutions with Al

In addition to the materials and solutions used in preparing pure CuO powder, an aluminum sulfate compound Al<sub>2</sub>(SO<sub>4</sub>)<sub>3</sub> is used as a source of Al in the doping process. At a concentration of 1%, 0.34 g of aluminum sulfate is added to 10 mL of deionized water and then mixed using a magnetic stirrer for 3 minutes at room temperature.

#### 2.3 Preparation of Al-doped CuO nanopowder

The aluminum sulfate solution is added to the prepared aqueous copper sulfate and sodium hydroxide solutions. The resulting mixture is placed on a heating plate at 100°C for 1 hour with magnetic stirring. The solution is then cooled, filtered, and dried at 100°C. Afterward, it is ground. The powder is divided into 6 samples and heated to the same previous temperatures (400°C, 450°C, 500°C,550°C, 600°C).

In order to determine the structure and size of the crystals in the prepared nanoparticles, XRD spectra of pure and Aldoped CuO samples are analyzed. XRD spectra are captured using the Bruker D8 Discover XRD device. The device specifications are as follows: target type: Cu-Kα; wavelength: 0.1540nm; current: 30mA; potential difference 40kV. The surface morphology of the prepared samples was studied using the USA Bruker Dimension Icon AFM device.

#### 3. Results and Discussion

#### 3.1 Structural properties

#### 3.1.1 XRD Analysis

The obtained spectra by Bruker D8 Discover XRD technique of pure CuO samples, before and after heat treatment at different temperatures, are shown in Fig. 2. The results are analyzed using the Origin Pro 9.1 program to determine the peak locations accurately. The peaks appear sharp when Xrays are directed at the CuO nanopowder, allowing them to overlap constructively when the Bragg conditions are met. As shown in Fig. 2, two clear peaks can be observed for all samples. The sharpness and intensity of the (002) and (200) peaks indicate that most of the planes have a preferred orientation in these directions, in addition to the presence of relatively weak peaks at different angles. These results are largely consistent with the international standard card with the serial number (JCPDS-05-0661). This confirms that the prepared samples have a polycrystalline and monoclinic structure, consistent with previous studies [8].

Fig. 3 shows that the Al element did not appear in the X-ray spectrum due to the low doping level. Only peaks related to CuO are observed. By comparing the obtained spectra at different temperatures of pure and Al-doped CuO, a slight shift of the peak positions towards higher 2θ shown in Fig. 3 for the doped nanopowder. In addition, peak intensity is increased relative to pure CuO nanopowder.

The shift in peak position and change in intensity can be attributed to an alteration in crystal symmetry due to the formation of vacancies and dislocations in the crystalline structure due to doping. These defects cause charge imbalance due to Al doping at Cu lattice sites [9].

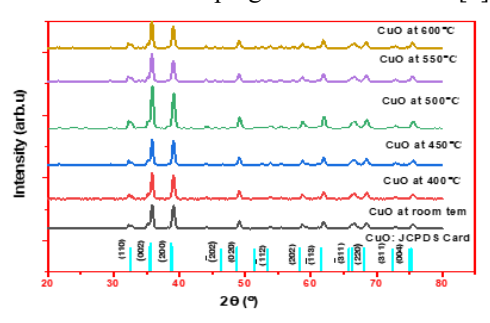
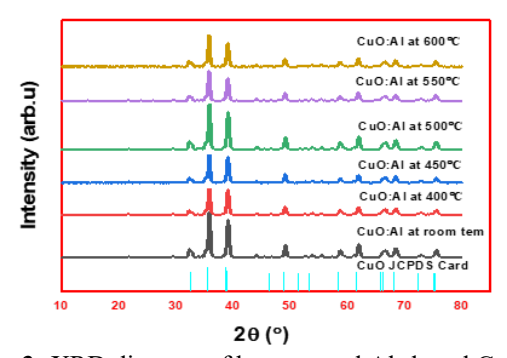


Fig. 2: XRD diagram of pure heat-treated CuO powder.



**Fig. 3:** XRD diagram of heat-treated Al-doped CuO powder.

#### 3.1.2 Calculation of synthetic coefficients

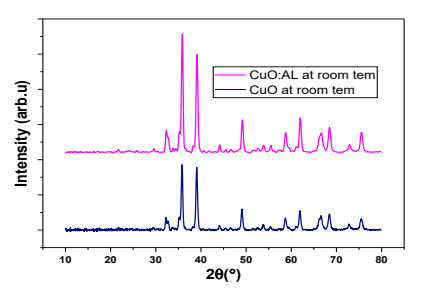
The crystallographic parameters, such as lattice parameters, interplanar distance, crystallite size, and dislocation density, were extracted by analyzing the data obtained from XRD analysis using the indicated relations [10,11]:

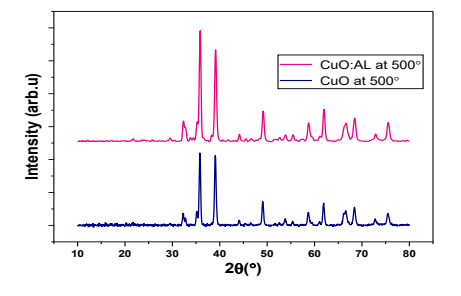
The lattice constants a, b, c,  $\beta$  of pure and CuO/Al powder are calculated using the relation:

$$\frac{1}{d^{2}} = \frac{1}{\sin^{2}\beta} \left[ \frac{h^{2}}{a^{2}} + \frac{k^{2}\sin^{2}\beta}{b^{2}} + \frac{l^{2}}{c^{2}} - \frac{2hl\cos\beta}{ac} \right]$$
(1)

Where d is the distance between crystal planes,  $\beta$  is the maximum width of the curve at the middle of the maximum intensity (FWHM) and measured in (rad), a, b, and c are

lattice parameters, 
$$k = \sqrt{\frac{4 \ln 2}{\pi}} = 0.94$$





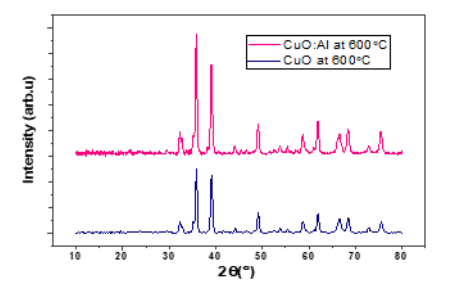


**Fig. 4:** Showing intensity difference of the peaks between the pure and Al-doped CuO samples at different temperatures.

Table 1 shows the values of the lattice constants for the pure and CuO/Al samples before and after heat treatment. It is noted that there is a close agreement between the theoretical lattice constants obtained from the JCPDS card and the experimentally obtained values for the pure CuO sample. However, a slight reduction in the lattice parameters (a, b, c)

is observed in both cases after heat treatment, indicating that heat treatment affects the lattice parameters.

The distance between the crystal planes is calculated using Bragg's law for the preferred orientations of crystallization (002), (200), (202), and (113).

$$2d_{hkl}\sin\theta = \lambda$$
 (2)

Where  $\lambda$  is the incident photon wavelength,  $\theta$  is the diffraction angle, dhkl is the inter distance, h, k, l are Miller indices. The calculated values of dhkl are shown in Tables 2 and 3, and indicate that dhkl is decreased with increasing annealing temperatures in pure CuO samples. However, dhk did not change in the doped samples.

**Table 1:** Lattice parameters values for pure and CuO/Al treated thermally at different temperatures.

Sample type	Temp.	a (A°)	b (A°)	C (A°)	β (A°)
JCPDS:05- 0661	Room temp.	4.684	3.425	5.129	99.47
Pure CuO	-	4.661	3.407	5.126	96.24
	400 °C	4.675	3.433	5.086	99.88
	450 °C	4.669	3.423	5.096	99.48
	500 °C	4.669	3.261	5.078	99.44
	550 °C	4.665	3.448	5.085	99.48
	600 °C	4.653	3.467	5.075	99.48
CuO/Al	Room temp.	4.666	3.461	5.076	99.49
	400 °C	4.665	3.461	5.076	99.49
	450 °C	4.665	3.461	5.076	99.49
	500 °C	4.661	3.465	5.071	99.46
	550 °C	4.667	3.433	5.078	99.45
	600 °C	4.667	3.433	5.078	99.45

The crystallite size is calculated from width to half height  $(\beta)$  based on Debey-Scherer's formula [11]:

$$D = k\lambda / \beta \cos\theta \tag{3}$$

D values of pure and doped powder at different temperatures are shown in Tables 2 and 3. It can be noted that the crystallite size of both pure and doped samples does not exceed 23.47nm, indicating that the prepared powders have a nanostructure. Table 2 shows that increasing the temperature of the pure sample up to 600 °C reduced the average crystallite size from 23.47 nm to 19.43 nm.

Moreover, Al doping caused a reduction in the crystallite size at room temperature to 19.92 nm. On the other hand, increasing the thermal treatment of the doped samples led to an increase in crystallite size to 20.95 nm, as indicated in Table 3.

To observe the effect of Al doping and heat treatment on the crystallite size of the prepared nanoparticles, the calculated values as a function of temperature are presented in Fig. 5. Fig. 5 shows that the crystallite size of nanoparticles is influenced by Al ion additions in the crystal lattice. Al doing reduced crystallite size which agrees with previous studies [12]. This confirms the replacement of Cu<sup>+2</sup> ions by

Al<sup>+3</sup> ions. This reduction in crystallite size is almost caused by a slight rise in the strain [12].

**Table 2:** XRD coefficients for pure CuO samples

Тетр.	Level (hkl)	$d_{hkl} \ (A^\circ)$	Peak Positio n 20()	FWHM β()	Crystal Size D(nm)	Average Crystal Size D(nm)
Room temp.	002	2.548	35.19	0.395	22.02	23.47
	200	2.317	38.82	0.401	21.93	
	-202	1.872	48.56	0.361	25.20	
	-113	1.494	62.05	0.391	24.75	
	002	2.505	35.81	0.394	22.12	22.61
400°C	200	2.303	39.07	0.434	20.27	
	-202	1.865	48.76	0.376	24.21	
	-113	1.498	61.82	0.405	23.87	
	002	2.513	35.70	0.389	22.39	23.12
450 °C	200	2.303	39.07	0.431	20.41	
	-202	1.854	49.07	0.370	24.64	
	-113	1.497	61.9	0.386	25.05	
	002	2.505	35.81	0.374	23.30	23.4
500°C	200	2.303	39.028	0.394	22.33	
	-202	1.853	49.08	0.373	24.44	
	-113	1.479	61.91	0.411	23.53	
550°C	002	2.508	35.76	0.409	20.22	22.60
	200	2.301	39.10	0.374	23.53	
	-202	1.853	49.10	0.397	22.96	
	-113	1.496	61.94	0.408	23.70	
600°C	002	2.503	35.83	0.427	20.41	
	200	2.295	39.20	0.486	18.11	19.43
	-202	1.854	49.07	0.457	19.95	
	-113	1.496	61.94	0.502	19.26	

Moreover, an increase in crystallite size values with increasing heat treatment up to 500  $^{\circ}\mathrm{C}$  is observed for pure samples, followed by a reduction with increasing temperature to 600  $^{\circ}\mathrm{C}$ . This variation corresponds to the opposite behavior in FWHM ( $\beta$ ), as shown in Fig. 6. The increase in particle size can be explained by the phenomenon of recrystallization under the influence of increasing annealing temperature.

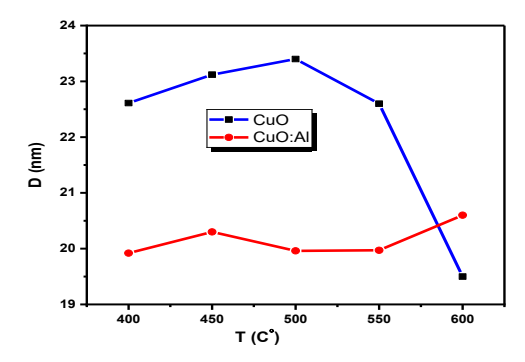
This means that the resulting CuO powder is well crystallized at 500 °C. A slight change in the crystalline size of the doped samples with rising temperatures is observed. These slight changes can be attributed to distortions resulting from the annealing process, which affected the crystallization of the sample.

The dislocation density  $\delta$  can be defined as the measurement of dislocation lines per unit volume of crystal and is calculated by the equation:

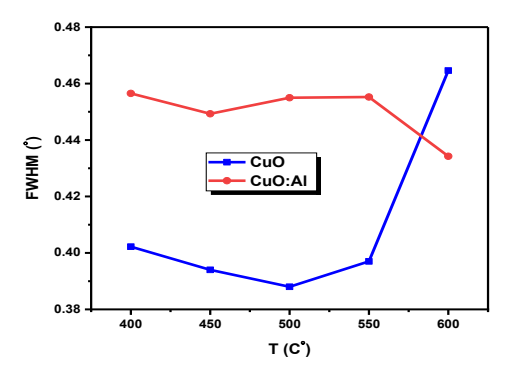
$$\delta = 1/D^2 \tag{4}$$

Table 3: XRD coefficients of Al-doped CuO samples.

Тетр.	Level (hkl)	d <sub>hki</sub> (A°)	Peak Position 2⊖(°)	FWHM β(˚)	Crystal Size D(nm)	Average Crystal Size D(nm)
Room temp.	002	2.503	35.83	0.437	19.94	
	200	2.301	39.09	0.457	19.26	19.92
	-202	1.853	49.10	0.429	21.26	
	-113	1.496	61.94	0.503	19.23	
	002	2.503	35.83	0.437	19.94	
400 °C	200	2.302	39.09	0.457	19.25	19.92
400 C	-202	1.853	49.10	0.429	21.25	
	-113	1.496	61.94	0.503	19.23	
450 °C	002	2.503	35.83	0.405	21.52	
	200	2.302	39.09	0.437	20.14	21.00
430 C	-202	1.853	49.10	0.408	22.34	
	-113	1.496	61.94	0.483	20.02	
	002	2.501	35.86	0.429	20.32	
500 °C	200	2.299	39.13	0.469	18.76	19.96
	-202	1.851	49.16	0.444	20.54	
	-113	1.495	61.98	0.478	20.24	
550 °C	002	2.505	35.79	0.419	20.80	
	200	2.302	39.07	0.466	18.88	19.97
	-202	1.853	49.08	0.444	20.53	
	-113	1.496	61.91	0.492	19.65	
600°C	002	2.505	35.79	0.391	22.29	
	200	2.303	39.06	0.447	19.68	20.95
600 C	-202	1.853	49.08	0.426	21.40	
	-113	1.496	61.91	0.473	20.44	



**Fig. 5:** Crystallite size variations in terms of annealing temperature of pure and doped samples.



**Fig. 6:** FWHM variations in terms of annealing temperature – of pure and doped samples.

At room temperature,  $\delta$  is lower for pure samples than doped ones. As temperature rises, ion displacement causes dislocations, increasing  $\delta$ . For doped samples, high temperatures trigger CuO molecule recrystallization, reducing  $\delta$ , as shown in Table 4.

**Table 4:** Dislocation density of pure and Al-doped CuO nanoparticles treated at different temperatures.

Annealing temp.	CuO	CuO/Al	
Room temp.	18.15	25.19	
400 °C	19.56	25.20	
450 °C	18.70	22.65	
500 °C	18.26	25.08	
550 °C	19.57	25.07	
600 °C	26.48	22.76	

#### 3.2 Morphological properties

#### 3.2.1 AFM Analysis

AFM images of the prepared samples are collected using USA Bruker Dimension Icon AFM. The obtained images are shown in Fig. 7. The examined samples at various angles revealed the formation of nanorods within the material. The transformation sequence of these structures begins with semi-oval nanoparticles, progresses to cylindrical nanoparticles or nanorods, and ultimately develops into cylindrical nanowires with increasing thermal treatment in the pure CuO samples starting at 500 °C, which resemble nanotubes. The length of the nanowires is observed to increase with rising annealing temperatures, accompanied by

a reduction in their thickness, with the thickness being below 20 nm and their length above 200 nm at 600 °C. This means that the lengths of the obtained CuO nanoparticles exceed similar nanoparticles reported in previous studies [13,14]. Furthermore, the grown nanowires or nanotubes are almost oriented parallel to each other.

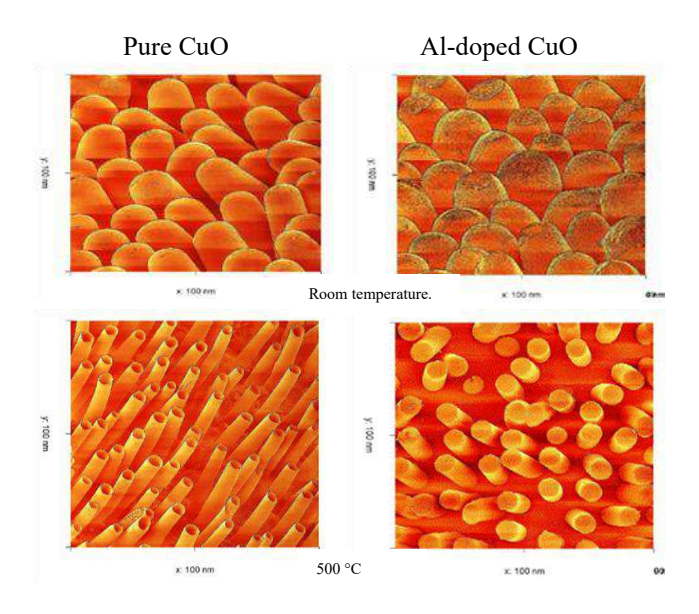


**Fig. 7:** AFM images of pure CuO nanoparticles to the left and CuO/Al to the right annealed at different temperatures.

A comparison of the AFM images of pure CuO and doped CuO/Al nanoparticles demonstrated distinct structural differences. While the doped CuO/Al nanorods appeared as solid nanorods at all temperatures, images showed a change in the morphology structure of pure samples to appear as nanotubes after thermal oxidation starting from 500 °C, as shown in Fig. 7. The formed nanotubes appear more clearly in Fig. 8. This behavior can be attributed to Kirkendall effect [1,15], in which atoms exchange with vacancies.

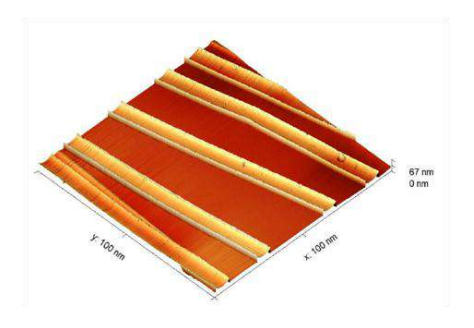


**Fig. 8:** AFM image of pure CuO nanoparticles showing clearly the hollow nanotubes after annealing at 600 °C.

The conversion process initiates with the adsorption of oxygen onto the surface of the nanowire. As the temperature

increases, Cu atoms predominantly diffuse outward, while the adsorbed oxygen atoms diffuse inward. The rate of Cu diffusion outward significantly exceeds the rate of oxygen diffusion inward [14], leading to the formation of vacancies during oxidation. Ultimately, this process results in the formation of hollow oxide nanostructures. In addition, the rapid thermal annealing has led to uniform wall thickness. This study demonstrates the ease with which metal oxide nanorods can be transformed into nanotubes through thermal oxidation under ambient air conditions.

Additionally, from a top-view perspective, the nanorods exhibited a circular morphology in both cases, as illustrated in Fig. 9.

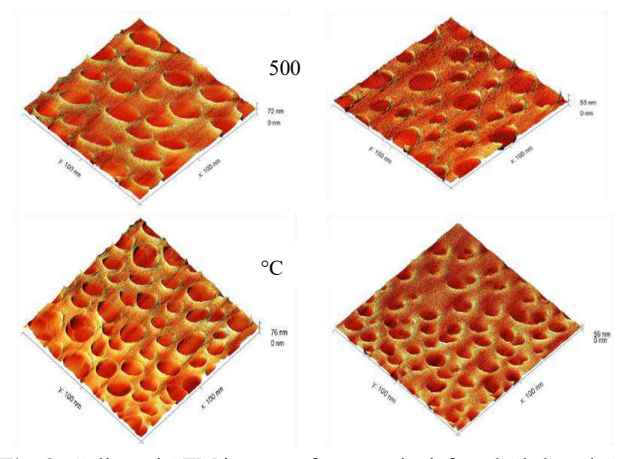


**Fig. 9:** Collected AFM images of pure to the left and Al-doped CuO nanostructures to the right at different tilt investigation angles.

#### 4. Conclusion

In this study, pure and Al-doped CuO nanoparticles were synthesized using the sol-gel method and subjected to thermal treatments. XRD analysis confirmed that both pure and doped CuO powders have a monoclinic crystal structure. Annealing led to slight reductions in lattice parameters. Dislocation density increased in pure CuO but decreased in the doped samples with higher temperatures.

AFM analysis showed the formation of nanorods or nanotubes. Rapid thermal annealing of CuO led to the formation of CuO nanotubes with uniform wall thickness and direction.

#### Acknowledgments

The authors of this research extend their sincere thanks and appreciation to Misurata University, where the samples were prepared in the research lab of the Chemistry Department, Faculty of Science.

**Conflict of interest**: The authors certify that there are no conflicts of interest.

#### 5. References

[1] M. Lai, S. Mubeen, N. Chartuprayoon, A. Mulchandani, M. A. Deshusses, and N. V. Myung, Synthesis of Sn doped CuO

nanotubes from core-shell Cu/SnO2 nanowires by the Kirkendall effect, J. Nanotechnol. 21(29), (2010) 295601. https://doi.org/10.1088/0957-4484/21/29/295601.

- [2] F. Bayansal, Y. Gülen, B. Şahin, S. Kahraman and H. A. Çetinkara, CuO nanostructures grown by the SILAR method: influence of Pb-doping on the morphological, structural and optical properties. J Alloys & Compounds. 619 (2015) 378–382. https://doi.org/10.1016/j.jallcom.2014.09.085.
- [3] S. Saleem, A. Khalid, Z. M. Aldhafeeri, A. Thamer, A. Arshad, M. AbdulJabbar, Y. Begum and G. Kandasamy, A comparative analysis of optical and electrical properties of pure CuO and Zn doped CuO nanoparticles for optoelectronic device applications. J Sol-Gel Sci Technol. 113 (2025) 213–224. https://doi.org/10.1007/s10971-024-06591-71
- [4] M. Arfana, D. N. Siddiquia, T. Shahidb, Z. Iqbala, Y. Majeeda, I. Akrama, Noreena, R. Bagherib, Z. Song and A. Zeb, Tailoring of nanostructures: Al doped CuO synthesized by composite hydroxide-mediated approach, Results in Physics, 13(2019), 102187.

#### https://doi.org/10.1016/j.rinp.2019.102187

- [5] R. M. Mohamed, F. A. Harraz and A. Shawky, CuO nanobelts synthesized by a template-free hydrothermal approach with optical and magnetic characteristics. Ceram Int. 40 (2014) 2127-2133. https://doi.org/10.1016/j.ceramint.2013.07.129
- [6] M. Ponnar, C. Thangamani, P. Monisha, S. S. Gomathi and K. Pushpanathan, Influence of Ce doping on CuO nanoparticles synthesized by microwave irradiation method. Appl Surf Sci. 449 (2018)132–143.

#### https://doi.org/10.1016/j.apsusc.2018.01.126

[7] H. Mersian, M. Alizadeh and N. Hadi, Synthesis of zirconium doped copper oxide (CuO) nanoparticles by the Pechini route and investigation of their structural and antibacterial properties. Ceram Int. 44 (2018) 20399–20408.

#### https://doi.org/10.1177/ 1847980418761775

[8] C. Thangamani, M. Ponnar, P. Priyadharshini, P. Monisha, S. Gomathi and K. Pushpanathan, Magnetic behavior of Ni-doped CuO nanoparticles synthesized by microwave radiation method. Surf. Rev. Lett. 26 (2018) 1-11.

#### https://doi.org/10.1142/s0218625x18501846.

[9] P. M. Shafi and A. C. Bose, Impact of crystalline defects and size on X-ray line broadening: A phenomenological approach for tetragonal SnO2 nanocrystals. AIP Adv. 5 (2015) 057137

#### https://doi.org/10.1016/j.colsurfa.2016.03.022.

- [10] K. Khashan, J. A. Saimon and A. A. Hassan, Optical Properties of CuO Thin Films with Different Concentration by Spray Pyrolysis Method, Eng. and Tech. J. 32(2014) 86-93
- [11] G. Abdulnabi and A. M. Juda, Preparation and characterization of (CuO/TiO2/ $\alpha$ -Fe2O3) ternary nanocomposite and application in a solar cell, J. Kufa Physics. 1(2023) 1-13. https://doi.org/10.31257/2018/JKP/2023/1501
- [12] R. Daira, B. Boudjema, M. Bououdina, MS. Aida, Influence of Al Doping on the Physical Properties of CuO Thin Films. Applied Sciences. 13(2023), 8193.

#### https://doi.org/10.3390/app13148193

- [13] M. Yousefi and C. Karami, The synthesis of CuO nanoparticles and investigating its effect at different temperature, Advances in Environmental Biology, (2014). 2113-2117.
- [14] R. S. Mohammed, K. A. Aadim, K. A. Ahmed, Synthesis of CuO/ZnO and MgO/ZnO core/shell nanoparticles with plasma jets and study of their structural and optical properties, Karbala Int. J. Mod. Sci. 8 (2022) 88e97,

#### https://doi.org/10.33640/2405-609X.3225.

[15] A. A. El Mel, R. Nakamura, C. Bittencourt, The Kirkendall effect and nanoscience: hollow nanospheres and nanotubes, J. Nanotechnol. 2015, 6, 1348–1361.

https://doi.org/10.3762/bjnano.6.139